


Origin of the insulating state in the honeycomb iridate Cu_2IrO_3

Ying Li ^{1,*}, Roger D. Johnson ², Yogesh Singh ³, Radu Coldea ⁴, and Roser Valentí ^{5,†}

¹*Department of Applied Physics and MOE Key Laboratory for Nonequilibrium Synthesis and Modulation of Condensed Matter, School of Physics, Xi'an Jiaotong University, Xi'an 710049, China*

²*Department of Physics and Astronomy, University College London, Gower Street, London WC1E 6BT, United Kingdom*

³*Indian Institute of Science Education and Research, Mohali, Sector 81, SAS Nagar, Manauli 140306, India*

⁴*Clarendon Laboratory, University of Oxford, Physics Department, Oxford OX1 3PU, United Kingdom*

⁵*Institut für Theoretische Physik, Goethe-Universität Frankfurt, Max-von-Laue-Strasse 1, 60438 Frankfurt am Main, Germany*



(Received 3 December 2024; revised 14 May 2025; accepted 19 May 2025; published 9 June 2025)

Through a combination of crystal symmetry analysis and density functional theory calculations we unveil a possible microscopic origin of the unexpected insulating behavior reported in the honeycomb Kitaev material Cu_2IrO_3 . Our study suggests that this material hosts an instability towards charge ordering of the Ir ions, with alternating magnetic Ir^{4+} and nonmagnetic Ir^{3+} ions arranged on the honeycomb lattice. In this case, the next-nearest-neighbor interactions that couple magnetic Ir^{4+} ions form an enlarged triangular lattice, instead of the expected honeycomb lattice. The magnetic Cu^{2+} ions located at the center of the iridium honeycomb voids also form a triangular lattice, and additionally contribute to the magnetization of the system. Together, the interpenetrated Ir^{4+} and Cu^{2+} triangular lattices present a novel type of honeycomb Kitaev lattice composed of two types of magnetic ion.

DOI: [10.1103/PhysRevB.111.245122](https://doi.org/10.1103/PhysRevB.111.245122)

I. INTRODUCTION

The iridate family $A_2\text{IrO}_3$ ($A = \text{Na}, \text{Li}$) has been considered as a prime candidate to realize the long-sought Kitaev \mathbb{Z}_2 spin liquid in a honeycomb lattice with nearest-neighbor bond-dependent Ising interactions [1–20]. However, the systems show long-range magnetic order due to the presence of further non-Kitaev interactions [21–25]. Attempts to modulate the magnetic couplings have been pursued by intercalation of H atoms [26–28] or Ag atoms [29] in $\alpha\text{-Li}_2\text{IrO}_3$. In the former, theoretical studies [30,31] indicated that H positions strongly affect the magnetic interactions [30] resulting in magnetic models with bond disorder. Such models in the presence of vacancies have been shown to reproduce the experimentally observed low-energy spectrum in $\text{H}_3\text{LiIr}_2\text{O}_6$ [32,33]. The iridate $\text{Ag}_3\text{LiIr}_2\text{O}_6$ was initially proposed to be closer to the Kitaev limit compared to $\alpha\text{-Li}_2\text{IrO}_3$, however, by improving the sample quality, the system shows long-range incommensurate antiferromagnetic (AFM) order [34,35]. In theoretical studies it was found that the Ir-O hybridization in $\text{Ag}_3\text{LiIr}_2\text{O}_6$ is moderate and a localized relativistic $j_{\text{eff}} = 1/2$ magnetic model with Kitaev and non-Kitaev exchange contributions is still valid for the description of the system [36], albeit its properties [37] may be affected by the presence of Ag vacancies [36,37]. A relatively new intercalated honeycomb system Cu_2IrO_3 has also been synthesized [38] consisting of Ir honeycomb layers, with Cu atoms situated both at the center

of the honeycomb voids, and in between the Ir layers as shown in Fig. 1(a).

A crystal structure with $C2/c$ space group symmetry was first proposed for this system, but it was later shown that three structures with the same qualitative atomic connectivity but different space group symmetries, $C2/c$, $C2/m$, and $P2_1/c$, could not be uniquely distinguished using the published powder x-ray diffraction data [39]. Susceptibility and specific heat measurements show that the system remains magnetically disordered until 2.7 K, at which point short-range order develops [38]. μSR measurements detect a two-component depolarization with slow- and fast-relaxation rates, attributed to coexistence of static and dynamic magnetism, with further evidence that both Ir^{4+} and Cu^{2+} magnetic moments exist [40]. Taken together, these magnetic properties were suggested to arise from significant levels of chemical disorder [41]. However, signatures characteristic of a Kitaev quantum spin liquid have also been reported based on nuclear quadrupole resonance and Raman scattering measurements [42,43]. Furthermore, Cu_2IrO_3 has been reported to show a complex set of structural phase transitions under hydrostatic pressure [39,44] and an insulator-to-metal transition [45]. More recently, Ref. [46] reported a $C2/m$ crystal structure with less antisite disorder between Cu and Ir ions in the honeycomb layers. In this publication magnetic susceptibility measurements revealed a weak ferromagnetic-like anomaly with hysteresis at a magnetic transition temperature of 70 K [46]. The crystal structures and bulk properties summarized above are consistent with linearly bonded, nonmagnetic Cu^+ ($3d^{10}$) ions located between honeycomb layers, and octahedrally coordinated, magnetic Cu^{2+} ($3d^9$) ions in the honeycomb voids. Charge is then balanced by a fractional oxidation state of

*Contact author: yingli1227@xjtu.edu.cn

†Contact author: valenti@itp.uni-frankfurt.de

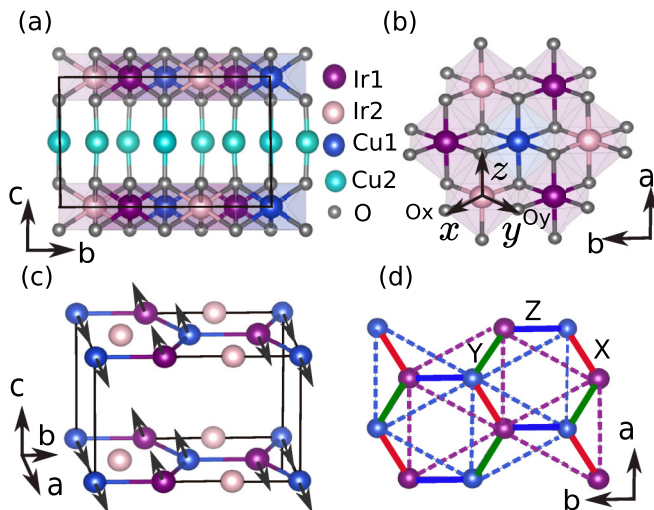


FIG. 1. Proposed charge-ordered crystal structure of Cu_2IrO_3 (C_2 symmetry) projected into (a) the bc and (b) the ab planes. The two nonequivalent Ir ions are labeled as Ir1 and Ir2. Cu1 and Cu2 indicate the copper ions in the honeycomb layer and between the layers, respectively. Ir1, Ir2 and Cu1 label single crystallographic sublattices, while Cu2 labels ions located on three symmetry-independent sublattices indicated as Cu2-1, Cu2-2, and Cu2-3 in Table IV in the Appendix. The average distances Ir1-O and Ir2-O are 2.04 \AA and 2.07 \AA , respectively. x, y, z are Cartesian axes used to describe the d orbitals of all Ir and Cu ions; x and y are defined with respect to the Ir2 octahedra, with the $\hat{x} + \hat{y}$ diagonal bisecting the $\text{O}_x\text{-Ir-O}_y$ bond angle and the $\hat{x} - \hat{y}$ diagonal along the twofold b axis. z then completes the right-handed orthonormal set, perpendicular to the xy plane. (c) The zigzag antiferromagnetic configuration used in the GGA + SO + U calculations. (d) Honeycomb lattice containing magnetic Cu1 (blue) and Ir1 (purple) ions. The Cu1-Ir1 distances are 3.11 \AA , and triangular lattices of magnetic Ir ions (Ir1) and Cu ions (Cu1) are shown by dashed lines. The Ir-Ir and Cu-Cu distances are 5.4 \AA .

$\text{Ir}^{3.5+}$ ($5d^{5.5}$), which would be expected to render the system metallic. It is hence an unresolved challenge to reconcile this expected metallic state with the experimentally observed insulating behavior at ambient pressure [38].

In this paper, we use symmetry considerations and density functional theory (DFT) to investigate the structural and electronic properties of Cu_2IrO_3 . We take as a starting point a C_2/m crystal structure, which is consistent with several other monoclinic layered honeycomb materials such as Na_2IrO_3 [11] and $\alpha\text{-Li}_2\text{IrO}_3$ [26]. Our structural relaxation and energy minimization results show that the insulating state in Cu_2IrO_3 may result from iridium charge ordering into magnetic Ir^{4+} ($5d^5$) and nonmagnetic Ir^{3+} ($5d^6$). The ideal magnetic ground state is therefore based on a honeycomb Kitaev lattice, composed not of nearest-neighbor Ir^{4+} ions, but of alternating Ir^{4+} and Cu^{2+} ions with nonmagnetic Ir^{3+} in the honeycomb voids.

II. CRYSTAL STRUCTURE

The crystal structure of Cu_2IrO_3 is composed of honeycomb layers formed from edge sharing IrO_6 octahedra, with Cu atoms occupying both the honeycomb voids (Cu1) and

the space between the layers (Cu2); see Fig. 1. We use as starting point a crystal structure with C_2/m symmetry derived from the C_2/c structure proposed in Ref. [38]. This model was further refined by performing a structural relaxation (see details below) in which the atomic fractional coordinates were allowed to vary, but the unit cell parameters were kept fixed to the experimental values [38] [the C_2/m unit cell (unprimed) is related to the C_2/c cell (primed) by the transformation $\mathbf{a} = -\mathbf{a}'$, $\mathbf{b} = -\mathbf{b}'$, $\mathbf{c} = (\mathbf{c}' + \mathbf{a}')/2$]. The resulting parameters are given on the right side of Table IV in the Appendix, and were found to be in good agreement with those of the C_2/m structure recently published in Ref. [46]. The octahedral coordination of the Cu1 sites is usually compatible with a Cu^{2+} valence state, while the linear bonding of the Cu2 sites is typical of a Cu^+ valence. This Cu charge configuration was confirmed by bond valence sum calculations performed on our relaxed C_2/m structure. We therefore discount the scenario of $\text{Cu}_2^{1+}\text{Ir}^{4+}\text{O}_3^{2-}$. Charge neutrality then implies an average iridium oxidation state of $+3.5$, i.e., a nominal composition $\text{Cu}_{0.5}^{2+}\text{Cu}_{1.5}^+\text{Ir}^{3.5+}\text{O}_3^{2-}$.

In C_2/m symmetry, the iridium ions are located on a single sublattice of symmetry-equivalent sites, so a fractional oxidation state of $+3.5$ for all iridium sites would be expected to lead to a metallic behavior. However, this fractional oxidation state also introduces an instability towards charge disproportionation, which would open an energy gap at the Fermi level giving rise to an insulator. Long-range charge order comprised of alternating nearest-neighbor Ir^{3+} and Ir^{4+} ions breaks both mirror and inversion symmetry. There is just one maximal subgroup of C_2/m compatible with this broken symmetry; C_2 . While other, lower symmetry subgroups may be realized, we limit our discussion to the highest symmetry case as is typical in the study of symmetry-breaking order. Any charge order will be accompanied by an ordered pattern of atomic displacements allowed within C_2 symmetry. In particular, one would expect to find small oxygen displacements that expand and contract the Ir^{3+} and Ir^{4+} octahedra, respectively.

To test the hypothesis of a charge ordered ground state we performed a structural relaxation within a model with C_2 symmetry using the Vienna *ab initio* simulation package (VASP) [47,48]. We considered relativistic effects as well as contributions of the Coulomb repulsion [49] $U_{\text{eff}} = U - J_H = 2.4 \text{ eV}$ for Ir ($U_{\text{eff}}^{\text{Ir}}$) following calculations for Na_2IrO_3 [50] and 8 eV for Cu ($U_{\text{eff}}^{\text{Cu}}$) following calculations for $\text{ZnCu}_3(\text{OH})_6\text{Cl}_2$ [51] within GGA + SO + U . We adopted a cutoff energy of 520 eV and a Monkhorst-pack $4 \times 2 \times 4$ k -points mesh. The structure was initialized with a nominal, symmetry-breaking distortion where the Ir1-O bond lengths were shortened on average (\bar{r}_s), and the Ir2-O bond lengths were lengthened on average (\bar{r}_l). The lattice parameters were fixed and the fractional coordinates of all ions were allowed to vary. The resultant structural parameters are given in the left side of Table IV in the Appendix (see also Fig. 1). The differences in relaxed Cu and Ir positions between the C_2/m reference structure and the C_2 structure were negligible, while the average Ir-O bond lengths were found to have a ratio of $\bar{r}_s/\bar{r}_l \sim 0.98$. The respective small shifts in oxygen positions are likely within the uncertainty of structural refinements against x-ray diffraction data, especially given the presence

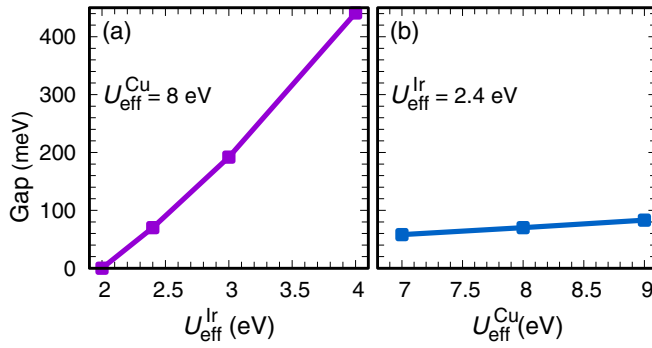


FIG. 2. Insulating gap in Cu_2IrO_3 as a function of (a) $U_{\text{eff}}^{\text{Ir}}$ ($U_{\text{eff}}^{\text{Cu}} = 8$ eV) and (b) $U_{\text{eff}}^{\text{Cu}}$ ($U_{\text{eff}}^{\text{Ir}} = 2.4$ eV) using GGA + SO + U with an antiferromagnetic configuration as shown in Fig. 1(c). $U_{\text{eff}}^{\text{Ir}}$ and $U_{\text{eff}}^{\text{Cu}}$ are the on-site Coulomb repulsion in Ir and Cu, respectively.

of stacking faults typically found in monoclinic layered honeycomb materials. However, our DFT calculations showed that the respective electronic properties are strongly affected, whereby the difference between the two iridium-oxygen coordinations induces a full charge order with nearest neighbor Ir^{4+} (Ir1) and Ir^{3+} (Ir2) ions. The total energy difference between $C2/m$ and $C2$ structural relaxations was only 4 meV per formula unit. Despite being close to the accuracy limit of our DFT calculations, this energy difference was found to be significant. Remarkably, such a small change in energy corresponded to complete charge order of the iridium ions, suggesting that slight perturbations may ultimately prevent long-range charge order in the real material. In this case the ground state could resemble a disordered, glassy array of Ir^{4+} and Ir^{3+} ions with their respective disordered oxygen displacements. We note that the average symmetry of the disordered ground state is $C2/m$, and therefore may be easily hidden in any diffraction experiment. For completeness, we also tested charge ordered structures based on the other two experimentally suggested symmetries ($P2_1/c$ and $C2/c$), and found robust charge order and insulating behavior in these symmetries.

III. ELECTRONIC PROPERTIES

The electronic properties were obtained from full-potential linearized augmented plane-wave (LAPW) calculations [52]. We chose the basis-size controlling parameter $\text{RK}_{\text{max}} = 7$ and a mesh of 500 \mathbf{k} points in the first Brillouin zone (FBZ) of the primitive unit cell. The density of states (DOS) were computed with 1000 \mathbf{k} points in the full Brillouin zone. An analysis of the insulating gap as a function of $U_{\text{eff}} = U - J_H$ was performed, having established that a zigzag antiferromagnetic configuration [see Fig. 1(c)] gave the lowest total energy compared to three other commensurate magnetic configurations (ferromagnetic, Néel, and stripy). As shown in Fig. 2, increasing $U_{\text{eff}}^{\text{Ir}}$ from 2–4 eV, the charge gap increases sharply from 0–0.44 eV. With increasing $U_{\text{eff}}^{\text{Cu}}$ from 7–9 eV, the gap increases slightly from 0.058–0.083 eV. The U_{eff} values for iridium atoms clearly affect the energy gap much more than those of copper.

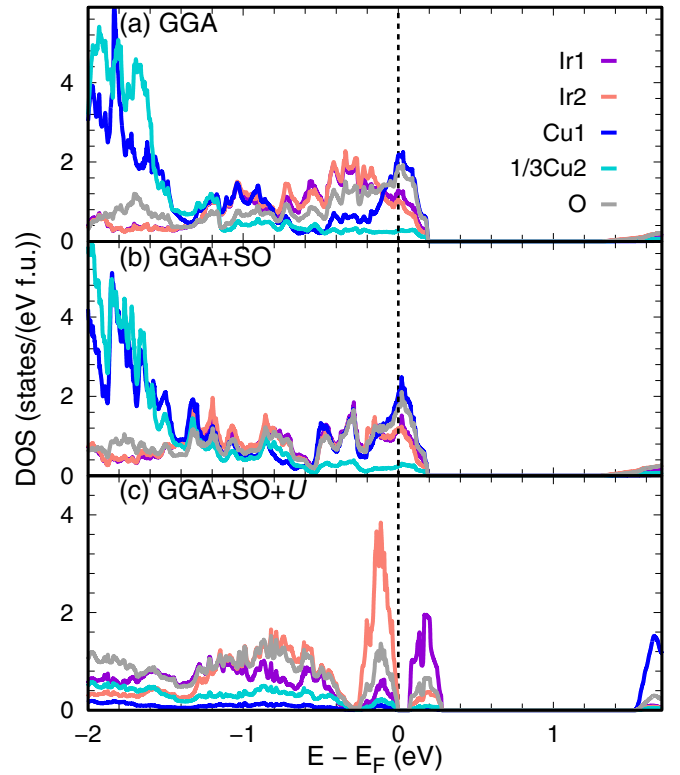


FIG. 3. Density of states obtained from (a) nonmagnetic GGA, (b) nonmagnetic GGA + SO, and (c) GGA + SO + U with the magnetic configuration displayed in Fig. 1(c). Note that the Cu2 DOS has been scaled by a factor 1/3.

In Fig. 3 we show the partial density of states (DOS) for the relaxed $C2$ structure obtained within nonmagnetic GGA and GGA + SO approximations, as well as GGA + SO + U assuming the zigzag antiferromagnetic configuration. In both the nonrelativistic GGA [Fig. 3(a)] and relativistic GGA + SO [Fig. 3(b)] partial DOS, Cu2 d states are almost fully occupied below the Fermi level, while Cu1 d states are partially occupied around the Fermi level. This result is consistent with Cu^+ at the Cu2 site and Cu^{2+} at the Cu1 site, as expected. The partial DOS of Ir1 and Ir2 differ in magnitude around the Fermi level, but have approximately the same form. As shown in Fig 3(c), including a Coulomb repulsion for Ir and Cu (GGA + SO + U) induces a charge order of Ir1 and Ir2, and opens a gap of about 70 meV (with $U_{\text{eff}} = U - J_H = 2.4$ eV [50]) for Ir and 8 eV for Cu. We note that GGA + U calculations without spin-orbit coupling, not shown here, converged to a metallic ferrimagnetic state where Ir1 has bigger moment than Ir2. Therefore, spin-orbit coupling, Coulomb repulsion, and magnetic moments on Ir are all important factors to stabilize the charge ordered state and the respective insulating behavior.

To further clarify the microscopic nature of the insulating state, we reevaluate the previously calculated GGA + SO + U Ir1 density of states projected onto a relativistic j_{eff} basis [Fig. 4(a)]. The Cu1 density of states was also projected onto a t_{2g} and e_g basis [Fig. 4(b)]. These data show that Ir1 has one hole in the $j_{\text{eff}} = 1/2$ state and Cu1 has one hole in the e_g orbital, both of which therefore contribute to the magnetism of the compound.

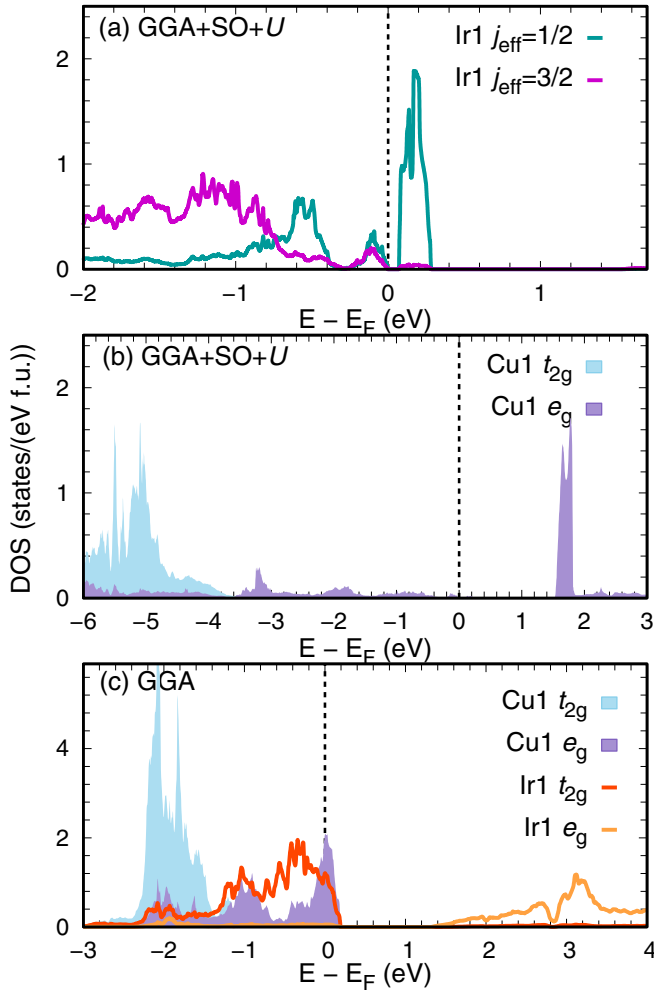


FIG. 4. The GGA + SO + U density of states projected onto (a) the relativistic j_{eff} basis of Ir1, and (b) the t_{2g} and e_g orbitals of Cu1. (c) Nonrelativistic GGA density of states projected onto t_{2g} and e_g orbitals for both Cu1 and Ir1.

IV. MAGNETIC PROPERTIES

We derived the magnetic exchange parameters using the projED method [23,53], which consists of the following two steps. First, *ab initio* hopping parameters between the Ir and Cu ions are extracted with projective Wannier functions [54] applied to nonrelativistic FPLO [55] calculations on a $10 \times 10 \times 10$ \mathbf{k} mesh. This allows us to construct an effective electronic model, $\mathcal{H}_{\text{tot}} = \mathcal{H}_{\text{hop}} + \mathcal{H}_{\text{SO}} + \mathcal{H}_U$, which includes the above calculated kinetic hopping term \mathcal{H}_{hop} , plus the spin-orbit coupling \mathcal{H}_{SO} and Coulomb interaction \mathcal{H}_U contributions. The spin-orbit coupling λ is set to 0.4 eV for Ir, and the Coulomb interactions were set to $U^{\text{Ir}} = 1.7$ eV, $J_{\text{H}}^{\text{Ir}} = 0.3$ eV, $U^{\text{Cu}} = 8$ eV, and $J_{\text{H}}^{\text{Cu}} = 1$ eV. We note that the Coulomb interaction value for Ir [23] considered in this effective Hubbard model is smaller than the one used in the GGA + U + SO calculations within the LAPW implementation, as we have explained in previous calculations [56]. In a next step, the effective spin Hamiltonian \mathcal{H}_{eff} is extracted from the electronic model via exact diagonalization (ED) of finite clusters. The projection of the resulting energy spectrum

TABLE I. Matrix elements of the crystal field Hamiltonian for Ir1 and Cu1 in units of meV, given in the t_{2g} , e_g basis defined with respect to the Cartesian axes xyz defined in Fig. 1(b). Values in bold indicate the dominant terms. The form of the Cu1 crystal field is consistent with its twofold site symmetry along the \hat{x} - \hat{y} direction. The Ir1 site has the same symmetry, and the additional zeros in the matrix Hamiltonian are likely due to the large energy gap between t_{2g} and e_g states.

	d_{xy}	d_{xz}	d_{yz}	d_{z^2}	$d_{x^2-y^2}$	
Ir1	d_{xy}	-542.4	-7.8	-7.8	0	0
	d_{xz}	-7.8	-548.7	-13.7	0	0
	d_{yz}	-7.8	-13.7	-548.7	0	0
	d_{z^2}	0	0	0	2665.7	0
	$d_{x^2-y^2}$	0	0	0	0	2689.1
	d_{xy}	-1884.1	-10.0	-10.0	71.0	0
Cu1	d_{xz}	-10.0	-1885.6	7.2	-116.4	0.1
	d_{yz}	-10.0	7.2	-1885.6	-116.4	-0.1
	d_{z^2}	71.0	-116.4	-116.4	-526.7	0
	$d_{x^2-y^2}$	0	0.1	-0.1	0	-543.3

onto the low-energy subspace is then obtained by adopting a pseudospin operator representation in the j_{eff} basis for Ir, and an e_g basis for Cu, with the projection operator defined as \mathbb{P} : $\mathcal{H}_{\text{eff}} = \mathbb{P}\mathcal{H}_{\text{tot}}\mathbb{P} = \sum_{ij} \mathbf{S}_i \mathbb{J}_{ij} \mathbf{S}_j$.

Considering only the magnetic ions Ir1 and Cu1, the nearest-neighbor interactions between Ir1 and Cu1 span bonds labeled X, Y, and Z [see Fig. 1(d)]. In the $C2$ space group symmetry, X and Y bonds are related by twofold rotation about the crystallographic b axis, and the Z bonds are independent. Strong hybridization of Ir and Cu was found in our calculations, which is consistent with the enhanced delocalization of $5d$ $j_{\text{eff}} = 1/2$ orbitals observed experimentally by resonant inelastic x-ray scattering [57]. The next-nearest-neighbor interactions are Ir1-Ir1 and Cu1-Cu1, which form two interpenetrating triangular lattices. The respective interaction distances are around 5.4 Å, much larger than the Ir1-Cu1 nearest-neighbor distance. Hence, in the following minimal model we only consider the hopping parameters between nearest neighbors Ir1 and Cu1.

The obtained crystal fields for Ir1 and Cu1 ions are shown in Table I. For the on-site orbital levels of Ir1 ions, e_g are empty above the Fermi level lying at 2.7 eV while t_{2g} are occupied at around -0.5 eV. For Cu1, the t_{2g} orbitals are fully occupied and located at around -1.9 eV while the e_g orbitals are found around -0.5 eV. These results are consistent with the GGA density of states presented in Fig. 4(c). Therefore the orbitals related to the electronic and magnetic properties close to the Fermi level are t_{2g} orbitals of Ir1 and e_g orbitals of Cu1.

The calculated, bond-dependent nearest-neighbor hopping parameters of Ir1-Cu1 bonds are given in Table II, again in the t_{2g} , e_g orbital basis. Different from Na_2IrO_3 and $\alpha\text{-Li}_2\text{IrO}_3$ where the involved orbitals for the three bonds are threefold symmetric, in the current system, due to Cu e_g orbitals, the hoppings are not threefold symmetric. For the Z-bond, hopping between Ir1 d_{xy} and Cu1 d_{z^2} was found to dominate, while for the X(Y) bond, the significant hopping contributions were between Ir1 d_{yz} (d_{xz}) and Cu1 d_{z^2} and $d_{x^2-y^2}$ orbitals.

TABLE II. Hopping parameters for Ir1-Cu1 nearest neighbor bonds, in units of meV, calculated for the X, Y, and Z bonds. Values in bold indicate the dominant terms. Note that the parameters found for X and Y bonds are consistent with the 2-fold rotational symmetry around $\hat{x}-\hat{y}$ that interrelates these two bonds.

		Cu1				
		d_{xy}	d_{xz}	d_{yz}	d_{z^2}	$d_{x^2-y^2}$
Ir1 (Z)	d_{xy}	13.1	-9.0	-9.0	231.1	0
	d_{xz}	-0.6	-11.8	-1.7	0.1	-28.8
	d_{yz}	-0.6	-1.7	-11.8	0.1	28.8
	d_{z^2}	0	0	0	0	0
	$d_{x^2-y^2}$	0	0	0	0	0
Ir1 (Y)	d_{xy}	-9.6	-5.6	-1.8	46.3	10.4
	d_{xz}	-0.7	11.6	13.5	-109.1	-196.6
	d_{yz}	-1.9	2.8	-9.8	-21.9	32.0
	d_{z^2}	0	0	0	0	0
	$d_{x^2-y^2}$	0	0	0	0	0
Ir1 (X)	d_{xy}	-9.6	-1.8	-5.6	46.3	-10.4
	d_{xz}	-1.9	-9.8	2.8	-21.9	-32.0
	d_{yz}	-0.7	13.5	11.6	-109.1	196.6
	d_{z^2}	0	0	0	0	0
	$d_{x^2-y^2}$	0	0	0	0	0

The resulting effective Hamiltonian can be written as:

$$\mathcal{H}_{\text{spin}} = \sum_{\langle ij \rangle} \mathbf{S}_i \cdot \mathbf{J}_{ij} \cdot \mathbf{S}_j, \quad (1)$$

where $\langle ij \rangle$ denotes a sum over all pairs of nearest-neighbor sites. In Kitaev's original honeycomb model, the exchange parameters are bond dependent. For example, the Z-bond interaction can be written as

$$\mathbf{J}^Z = \begin{pmatrix} J + \xi & \Gamma & \Gamma' + \zeta \\ \Gamma & J - \xi & \Gamma' - \zeta \\ \Gamma' + \zeta & \Gamma' - \zeta & J + K \end{pmatrix}. \quad (2)$$

The calculated exchange parameters for all three bonds are given in Table III. For the Z bond this magnetic model has a large negative Heisenberg J and a positive Kitaev K term; both of those terms change sign and reduce in magnitude for the X and Y bonds. The magnetic model is not threefold symmetric due to the anisotropy of the hoppings.

A mean-field calculation using SPINW [58] finds that this Hamiltonian has a Néel-type magnetic order in the ground state, which differs from the zigzag order found in our DFT total energy calculations. We suggest that this discrepancy may come from the presence of significant magnetic interactions beyond the minimal nearest-neighbor model in (1), such as antiferromagnetic next-nearest-neighbor couplings, which would favor zigzag order. Further neighbor couplings in other

TABLE III. Calculated nearest-neighbor exchange parameters in units of meV.

Bond	J	K	Γ	Γ'	ξ	ζ
Z	-16.1	34.1	1.6	-0.1	0.0	0.0
X, Y	9.4	-18.9	-0.7	2.2	1.1	-4.7

Kitaev candidate materials, for instance Na_2IrO_3 , change indeed the nature of the magnetic state [23]. Similar to Ref. [23], the exchange parameters could also be affected by the values of U , J_H , and λ in the calculations. Here we used the standard parameters for Ir and Cu. Since Cu_2IrO_3 is more complex than Na_2IrO_3 and $\alpha\text{-Li}_2\text{IrO}_3$ due to the presence of the various Cu and Ir oxidation states, this increase in parameter-space possibilities results in very heavy calculations, both at the ED and DFT level. ED calculations would require the consideration of larger clusters, while DFT calculations would require considering noncollinear configurations. Due to the complexity of the present system with two different magnetic ions, these calculations are left for future studies.

V. SUMMARY

In summary, we have shown through a combination of symmetry analysis, structural relaxations, and electronic structure calculations that the experimentally observed insulating behavior in Cu_2IrO_3 can originate in the charge ordering of iridium ions. In this scenario, nonmagnetic Ir^{3+} and magnetic Ir^{4+} ions alternate on the iridium honeycomb lattice. In addition to the insulating behavior observed in resistivity experiments, a possible experimental verification can be obtained from x-ray absorption near edge structure (XANES), resonant inelastic x-ray scattering (RIXS), x-ray photoemission spectroscopy (XPS), and core-level electron energy loss spectroscopy (EELS). XANES for K edge Cu could verify two distinct Cu ions, Cu^{2+} and Cu^{1+} in Ref. [40] and Ref. [57]. XANES of L_3 edge Ir was explained as Ir^{4+} in Ref. [57]. However, the peaks positions of Ir^{4+} and Ir^{3+} are close [59], therefore it is difficult to distinguish them. RIXS reported in Ref. [57] at ambient pressure show clear $j_{1/2}$ transitions. However, both pure Ir^{4+} and charge order from (Ir^{4+} , Ir^{3+}) could capture these transitions. The experiment shows a broad peak around 0.6 eV, which is different from the features observed in Na_2IrO_3 and $\alpha\text{-Li}_2\text{IrO}_3$ [13] where Ir is in a Ir^{4+} oxidation states. In these compounds exciton peaks were observed at 0.42–0.45 eV, and 0.72–0.83 eV. The differences in peak positions between Cu_2IrO_3 and the latter compounds indicate deviations from a pure Ir^{4+} response in the former. Further analysis both from RIXS experiments and theory are left for future study. Similar charge order effects have been observed in $\text{K}_{0.5}\text{RuCl}_3$ [60], with magnetic Ru^{3+} and nonmagnetic Ru^{2+} populating the transition-metal honeycomb. XPS and EELS experiments, having been used to measure a charge order in $\text{K}_{0.5}\text{RuCl}_6$, could also be used to probe Cu_2IrO_3 . Distinct from the $\text{K}_{0.5}\text{RuCl}_3$ case, we show that in Cu_2IrO_3 magnetic Cu^{2+} ions are located in the iridium honeycomb voids, contributing to a novel, composite $\text{Cu}^{2+}\text{-Ir}^{4+}$ -Kitaev honeycomb lattice that includes $3d\ s = 1/2$ and $5d\ j_{\text{eff}} = 1/2$ magnetic moments. We note that the associated lattice distortions are small, and may be easily missed in diffraction experiments. Both our DFT and model spin Hamiltonian calculations support an antiferromagnetic ground state that has not been observed. However, the total energy gained by charge order is relatively small, suggesting that long-range charge order, and the respective magnetic order, is vulnerable to perturbation.

ACKNOWLEDGMENTS

Y.L. acknowledges support from the National Natural Science Foundation of China (Grant No. 12004296) and Fundamental Research Funds for the Central Universities (Grant No. xzy012023051). R.V. acknowledges support from the Deutsche Forschungsgemeinschaft (DFG, German Research

Foundation) for funding through TRR 288 – 422213477 (project A05) and through VA 117/23-1 – 509751747. R.C. acknowledges support from the European Research Council under the European Union’s Horizon 2020 Research and Innovation Programme Grant Agreement No. 788814 (EQFT).

APPENDIX: STRUCTURAL PARAMETERS OF Cu_2IrO_3

In this Appendix we provide full crystallographic details for the $C2$ charge ordered and $C2/m$ reference crystal structures discussed in the main text.

TABLE IV. Crystallographic details for the $C2$ charge ordered structure (left) derived from the $C2/m$ reference structure (right) refined by *ab initio* structural relaxation. The subgroup basis is $\{[1,0,0],[0,1,0],[0,0,1]\}$, origin = $[0,0,0]$ with respect to the reference structure. Rows are spaced to indicate the relationship between sites of both structures (e.g., site Cu2-2 of $C2/m$ splits into sites Cu2-2 and Cu2-3 of $C2$, while site Cu2-1 does not split). The lattice parameters are common to both structures.

Space group $C2$ (No. 5)					Space group $C2/m$ (No. 12)				
$a = 5.393 \text{ \AA}, b = 9.311 \text{ \AA}, c = 5.961 \text{ \AA}, \beta = 107.506^\circ$									
Atom	Wyckoff	x	y	z	Atom	Wyckoff	x	y	z
Ir1	2a	0	0.33386	0	Ir	4g	0	0.33328	0
Ir2	2a	0	0.66615	0					
Cu1	2a	0	0.00000	0	Cu1	2a	0	0	0
Cu2-1	2b	0	0.49718	0.5	Cu2-1	2d	0	0.5	0.5
Cu2-2	2b	0	0.18094	0.5	Cu2-2	4h	0	0.17707	0.5
Cu2-3	2b	0	0.82302	0.5					
O1	4c	0.11950	0.49773	0.82439	O1	4i	0.10562	0.5	0.82306
O2	4c	0.10630	0.17343	0.81942	O2	8j	0.11005	0.16919	0.82254
O3	4c	0.38529	0.32896	0.18061					

- [1] A. Kitaev, Anyons in an exactly solved model and beyond, *Ann. Phys. (NY)* **321**, 2 (2006).
- [2] G. Jackeli and G. Khaliullin, Mott insulators in the strong spin-orbit coupling limit: From Heisenberg to a quantum compass and Kitaev models, *Phys. Rev. Lett.* **102**, 017205 (2009).
- [3] J. Chaloupka, G. Jackeli, and G. Khaliullin, Zigzag magnetic order in the iridium oxide Na_2IrO_3 , *Phys. Rev. Lett.* **110**, 097204 (2013).
- [4] W. Witczak-Krempa, G. Chen, Y. B. Kim, and L. Balents, Correlated quantum phenomena in the strong spin-orbit regime, *Annu. Rev. Condens. Matter Phys.* **5**, 57 (2014).
- [5] J. G. Rau, E. K.-H. Lee, and H.-Y. Kee, Spin-orbit physics giving rise to novel phases in correlated systems: Iridates and related materials, *Annu. Rev. Condens. Matter Phys.* **7**, 195 (2016).
- [6] R. Schaffer, E. K.-H. Lee, B.-J. Yang, and Y. B. Kim, Recent progress on correlated electron systems with strong spin-orbit coupling, *Rep. Prog. Phys.* **79**, 094504 (2016).
- [7] S. M. Winter, A. A. Tsirlin, M. Daghofer, J. van den Brink, Y. Singh, P. Gegenwart, and R. Valentí, Models and materials for generalized Kitaev magnetism, *J. Phys.: Condens. Matter* **29**, 493002 (2017).
- [8] S. Trebst, Kitaev materials, [arXiv:1701.07056](https://arxiv.org/abs/1701.07056).
- [9] G. Cao and P. Schlottmann, The challenge of spin-orbit-tuned ground states in iridates: a key issues review, *Rep. Prog. Phys.* **81**, 042502 (2018).
- [10] Y. Singh and P. Gegenwart, Antiferromagnetic mott insulating state in single crystals of the honeycomb lattice material Na_2IrO_3 , *Phys. Rev. B* **82**, 064412 (2010).
- [11] S. K. Choi, R. Coldea, A. N. Kolmogorov, T. Lancaster, I. I. Mazin, S. J. Blundell, P. G. Radaelli, Y. Singh, P. Gegenwart, K. R. Choi, S.-W. Cheong, P. J. Baker, C. Stock, and J. Taylor, Spin waves and revised crystal structure of honeycomb iridate Na_2IrO_3 , *Phys. Rev. Lett.* **108**, 127204 (2012).
- [12] Y. Singh, S. Manni, J. Reuther, T. Berlijn, R. Thomale, W. Ku, S. Trebst, and P. Gegenwart, Relevance of the Heisenberg-Kitaev model for the honeycomb lattice iridates A_2IrO_3 , *Phys. Rev. Lett.* **108**, 127203 (2012).
- [13] H. Gretarsson, J. P. Clancy, X. Liu, J. P. Hill, E. Bozin, Y. Singh, S. Manni, P. Gegenwart, J. Kim, A. H. Said, D. Casa, T. Gog, M. H. Upton, H.-S. Kim, J. Yu, V. M. Katukuri, L. Hozoi, J. van den Brink, and Y.-J. Kim, Crystal-field splitting and correlation effect on the electronic structure of A_2IrO_3 , *Phys. Rev. Lett.* **110**, 076402 (2013).
- [14] K. A. Modic, T. E. Smidt, I. Kimchi, N. P. Breznay, A. Biffin, S. Choi, R. D. Johnson, R. Coldea, P. Watkins-Curry, G. T. McCandless *et al.*, Realization of a three-dimensional spin-anisotropic harmonic honeycomb iridate, *Nature Commun.* **5**, 4203 (2014).
- [15] F. Freund, S. C. Williams, R. D. Johnson, R. Coldea, P. Gegenwart, and A. Jesche, Single crystal growth from separated

- educts and its application to lithium transition-metal oxides, *Sci. Rep.* **6**, 35362 (2016).
- [16] S. C. Williams, R. D. Johnson, F. Freund, S. Choi, A. Jesche, I. Kimchi, S. Manni, A. Bombardi, P. Manuel, P. Gegenwart, and R. Coldea, Incommensurate counterrotating magnetic order stabilized by Kitaev interactions in the layered honeycomb α -Li₂IrO₃, *Phys. Rev. B* **93**, 195158 (2016).
- [17] A. Biffin, R. D. Johnson, S. Choi, F. Freund, S. Manni, A. Bombardi, P. Manuel, P. Gegenwart, and R. Coldea, Unconventional magnetic order on the hyperhoneycomb Kitaev lattice in β -Li₂IrO₃: Full solution via magnetic resonant x-ray diffraction, *Phys. Rev. B* **90**, 205116 (2014).
- [18] A. Biffin, R. D. Johnson, I. Kimchi, R. Morris, A. Bombardi, J. G. Analytis, A. Vishwanath, and R. Coldea, Noncoplanar and counterrotating incommensurate magnetic order stabilized by Kitaev interactions in γ -Li₂IrO₃, *Phys. Rev. Lett.* **113**, 197201 (2014).
- [19] T. Takayama, A. Kato, R. Dinnebier, J. Nuss, H. Kono, L. S. I. Veiga, G. Fabbris, D. Haskel, and H. Takagi, Hyperhoneycomb iridate β -Li₂IrO₃ as a platform for Kitaev magnetism, *Phys. Rev. Lett.* **114**, 077202 (2015).
- [20] Y. Li, S. M. Winter, H. O. Jeschke, and R. Valentí, Electronic excitations in γ -Li₂IrO₃, *Phys. Rev. B* **95**, 045129 (2017).
- [21] V. M. Katukuri, S. Nishimoto, V. Yushankhai, A. Stoyanova, H. Kandpal, S. Choi, R. Coldea, I. Rousochatzakis, L. Hozoi, and J. van den Brink, Kitaev interactions between $j = 1/2$ moments in honeycomb Na₂IrO₃ are large and ferromagnetic: insights from *ab initio* quantum chemistry calculations, *New J. Phys.* **16**, 013056 (2014).
- [22] J. G. Rau, E. K.-H. Lee, and H.-Y. Kee, Generic spin model for the honeycomb iridates beyond the Kitaev limit, *Phys. Rev. Lett.* **112**, 077204 (2014).
- [23] S. M. Winter, Y. Li, H. O. Jeschke, and R. Valentí, Challenges in design of Kitaev materials: Magnetic interactions from competing energy scales, *Phys. Rev. B* **93**, 214431 (2016).
- [24] S. Ducatman, I. Rousochatzakis, and N. B. Perkins, Magnetic structure and excitation spectrum of the hyperhoneycomb Kitaev magnet β -Li₂IrO₃, *Phys. Rev. B* **97**, 125125 (2018).
- [25] I. Rousochatzakis and N. B. Perkins, Magnetic field induced evolution of intertwined orders in the Kitaev magnet β -Li₂IrO₃, *Phys. Rev. B* **97**, 174423 (2018).
- [26] M. J. O'Malley, P. M. Woodward, and H. Verweij, Production and isolation of pH sensing materials by carbonate melt oxidation of iridium and platinum, *J. Mater. Chem.* **22**, 7782 (2012).
- [27] S. Bette, T. Takayama, K. Kitagawa, R. Takano, H. Takagi, and R. E. Dinnebier, Solution of the heavily stacking faulted crystal structure of the honeycomb iridate H₃LiIr₂O₆, *Dalton Trans.* **46**, 15216 (2017).
- [28] K. Kitagawa, T. Takayama, Y. Matsumoto, A. Kato, R. Takano, Y. Kishimoto, S. Bette, R. Dinnebier, G. Jackeli, and H. Takagi, A spin-orbital-entangled quantum liquid on a honeycomb lattice, *Nature (London)* **554**, 341 (2018).
- [29] F. Bahrami, W. Lafargue-Dit-Hauret, O. I. Lebedev, R. Movshovich, H.-Y. Yang, D. Broido, X. Rocquefelte, and F. Tafti, Thermodynamic evidence of proximity to a Kitaev spin liquid in Ag₃LiIr₂O₆, *Phys. Rev. Lett.* **123**, 237203 (2019).
- [30] Y. Li, S. M. Winter, and R. Valentí, Role of hydrogen in the spin-orbital-entangled quantum liquid candidate H₃LiIr₂O₆, *Phys. Rev. Lett.* **121**, 247202 (2018).
- [31] R. Yadav, R. Ray, M. S. Eldeeb, S. Nishimoto, L. Hozoi, and J. van den Brink, Strong effect of hydrogen order on magnetic Kitaev interactions in H₃LiIr₂O₆, *Phys. Rev. Lett.* **121**, 197203 (2018).
- [32] J. Knolle, R. Moessner, and N. B. Perkins, Bond-disordered spin liquid and the honeycomb iridate H₃LiIr₂O₆: Abundant low-energy density of states from random Majorana hopping, *Phys. Rev. Lett.* **122**, 047202 (2019).
- [33] W.-H. Kao, J. Knolle, G. B. Halász, R. Moessner, and N. B. Perkins, Vacancy-induced low-energy density of states in the Kitaev spin liquid, *Phys. Rev. X* **11**, 011034 (2021).
- [34] F. Bahrami, E. M. Kenney, C. Wang, A. Berlie, O. I. Lebedev, M. J. Graf, and F. Tafti, Effect of structural disorder on the Kitaev magnet Ag₃LiIr₂O₆, *Phys. Rev. B* **103**, 094427 (2021).
- [35] J. Wang, W. Yuan, T. Imai, P. M. Singer, F. Bahrami, and F. Tafti, NMR investigation on the honeycomb iridate Ag₃LiIr₂O₆, *Phys. Rev. B* **103**, 214405 (2021).
- [36] Y. Li and R. Valentí, Role of disorder in electronic and magnetic properties of Ag₃LiIr₂O₆, *Phys. Rev. B* **105**, 115123 (2022).
- [37] A. de la Torre, B. Zager, F. Bahrami, M. DiScala, J. R. Chamorro, M. H. Upton, G. Fabbris, D. Haskel, D. Casa, T. M. McQueen, F. Tafti, and K. W. Plumb, Enhanced hybridization in the electronic ground state of the intercalated honeycomb iridate Ag₃LiIr₂O₆, *Phys. Rev. B* **104**, L100416 (2021).
- [38] M. Abramchuk, C. Ozsoy-Keskinbora, J. W. Krizan, K. R. Metz, D. C. Bell, and F. Tafti, Cu₂IrO₃: A new magnetically frustrated honeycomb iridate, *J. Am. Chem. Soc.* **139**, 15371 (2017).
- [39] G. Fabbris, A. Thorn, W. Bi, M. Abramchuk, F. Bahrami, J. H. Kim, T. Shinmei, T. Irifune, F. Tafti, A. N. Kolmogorov, and D. Haskel, Complex pressure-temperature structural phase diagram of the honeycomb iridate Cu₂IrO₃, *Phys. Rev. B* **104**, 014102 (2021).
- [40] E. M. Kenney, C. U. Segre, W. Lafargue-Dit-Hauret, O. I. Lebedev, M. Abramchuk, A. Berlie, S. P. Cottrell, G. Simutis, F. Bahrami, N. E. Mordvinova, G. Fabbris, J. L. McChesney, D. Haskel, X. Rocquefelte, M. J. Graf, and F. Tafti, Coexistence of static and dynamic magnetism in the Kitaev spin liquid material Cu₂IrO₃, *Phys. Rev. B* **100**, 094418(R) (2019).
- [41] Y. S. Choi, C. H. Lee, S. Lee, S. Yoon, W.-J. Lee, J. Park, A. Ali, Y. Singh, J.-C. Orain, G. Kim, J.-S. Rhyee, W.-T. Chen, F. Chou, and K.-Y. Choi, Exotic low-energy excitations emergent in the random Kitaev magnet Cu₂IrO₃, *Phys. Rev. Lett.* **122**, 167202 (2019).
- [42] S. K. Takahashi, J. Wang, A. Arsenault, T. Imai, M. Abramchuk, F. Tafti, and P. M. Singer, Spin excitations of a proximate Kitaev quantum spin liquid realized in Cu₂IrO₃, *Phys. Rev. X* **9**, 031047 (2019).
- [43] S. Pal, A. Seth, P. Sakrikar, A. Ali, S. Bhattacharjee, D. V. S. Muthu, Y. Singh, and A. K. Sood, Probing signatures of fractionalization in the candidate quantum spin liquid Cu₂IrO₃ via anomalous Raman scattering, *Phys. Rev. B* **104**, 184420 (2021).
- [44] S. Pal, P. Malavi, A. Sinha, A. Ali, P. Sakrikar, B. Joseph, U. V. Waghmare, Y. Singh, D. V. S. Muthu, S. Karmakar, and A. K. Sood, Pressure tuning of structure, magnetic frustration, and carrier conduction in the Kitaev spin liquid candidate Cu₂IrO₃, *Phys. Rev. B* **107**, 085105 (2023).

- [45] C. Jin, Y. Wang, M. Jin, Z. Jiang, D. Jiang, J. Li, Y. Nakamoto, K. Shimizu, and J. Zhu, Insulator-metal transition and crossover from negative to positive magnetoresistance in Cu_2IrO_3 under high pressure, *Phys. Rev. B* **105**, 144402 (2022).
- [46] Y. Haraguchi, D. Nishio-Hamane, A. Matsuo, K. Kindo, and H. A. Katori, High-temperature magnetic anomaly via suppression of antisite disorder through synthesis route modification in a Kitaev candidate Cu_2IrO_3 , *J. Phys.: Condens. Matter* **36**, 405801 (2024).
- [47] G. Kresse and J. Furthmüller, Efficiency of *ab-initio* total energy calculations for metals and semiconductors using a plane-wave basis set, *Comput. Mater. Sci.* **6**, 15 (1996).
- [48] J. Hafner, *Ab-initio* simulations of materials using vasp: Density-functional theory and beyond, *J. Comput. Chem.* **29**, 2044 (2008).
- [49] S. L. Dudarev, G. A. Botton, S. Y. Savrasov, C. J. Humphreys, and A. P. Sutton, Electron-energy-loss spectra and the structural stability of nickel oxide: An LSDA+U study, *Phys. Rev. B* **57**, 1505 (1998).
- [50] Y. Li, K. Foyevtsova, H. O. Jeschke, and R. Valentí, Analysis of the optical conductivity for A_2IrO_3 (A=Na, Li) from first principles, *Phys. Rev. B* **91**, 161101(R) (2015).
- [51] A. Pustogow, Y. Li, I. Voloshenko, P. Puphal, C. Krellner, I. I. Mazin, M. Dressel, and R. Valentí, Nature of optical excitations in the frustrated kagome compound herbertsmithite, *Phys. Rev. B* **96**, 241114(R) (2017).
- [52] P. Blaha, K. Schwarz, F. Tran, R. Laskowski, G. K. H. Madsen, and L. D. Marks, WIEN2k: An APW+lo program for calculating the properties of solids, *J. Chem. Phys.* **152**, 074101 (2020).
- [53] K. Riedl, Y. Li, R. Valentí, and S. M. Winter, *Ab initio* approaches for low-energy spin Hamiltonians, *Phys. Status Solidi B* **256**, 1800684 (2019).
- [54] H. Eschrig and K. Koepfner, Tight-binding models for the iron-based superconductors, *Phys. Rev. B* **80**, 104503 (2009).
- [55] K. Koepfner and H. Eschrig, Full-potential nonorthogonal local-orbital minimum-basis band-structure scheme, *Phys. Rev. B* **59**, 1743 (1999).
- [56] D. A. S. Kaib, K. Riedl, A. Razpopov, Y. Li, S. Backes, I. I. Mazin, and R. Valentí, Electronic and magnetic properties of the RuX_3 (X = Cl, Br, I) family: two siblings—and a cousin? *npj Quantum Mater.* **7**, 75 (2022).
- [57] G. Fabbris, E. H. T. Poldi, S. Sinha, J. Lim, T. Elmslie, J. H. Kim, A. Said, M. Upton, M. Abramchuk, F. Bahrami, C. Kenney-Benson, C. Park, G. Shen, Y. K. Vohra, R. J. Hemley, J. J. Hamlin, F. Tafti, and D. Haskel, Electronic structure of the honeycomb iridate Cu_2IrO_3 at high pressure, *Phys. Rev. B* **111**, 075153 (2025).
- [58] S. Toth and B. Lake, Linear spin wave theory for single-Q incommensurate magnetic structures, *J. Phys.: Condens. Matter* **27**, 166002 (2015).
- [59] J. P. Clancy, N. Chen, C. Y. Kim, W. F. Chen, K. W. Plumb, B. C. Jeon, T. W. Noh, and Y.-J. Kim, Spin-orbit coupling in iridium-based *5d* compounds probed by x-ray absorption spectroscopy, *Phys. Rev. B* **86**, 195131 (2012).
- [60] A. Koitzsch, C. Habenicht, E. Müller, M. Knupfer, B. Büchner, S. Kretschmer, M. Richter, J. van den Brink, F. Börrnert, D. Nowak, A. Isaeva, and T. Doert, Nearest-neighbor Kitaev exchange blocked by charge order in electron-doped $\alpha\text{-RuCl}_3$, *Phys. Rev. Mater.* **1**, 052001(R) (2017).